Intensity-Dependent Exciton Dynamics of (6,5) Single-Walled Carbon Nanotubes: Momentum Selection Rules, Diffusion, and Nonlinear Interactions

D. Mark Harrah,[†,‡,*] Jude R. Schneck,[¶,‡] Alexander A. Green,[§] Mark C. Hersam,[∥,⊥] Lawrence D. Ziegler,[¶,‡] and Anna K. Swan[†,#,‡,*]

[†]Department of Electrical and Computer Engineering, [‡]Photonics Center, [¶]Department of Chemistry, and [#]Department of Physics, Boston University, Boston, Massachusetts, [§]Wyss Institute, Harvard University, Cambridge, Massachusetts, and [∥]Department of Materials Science and Engineering, and [⊥]Department of Chemistry, Northwestern University, Evanston, Illinois

ABSTRACT

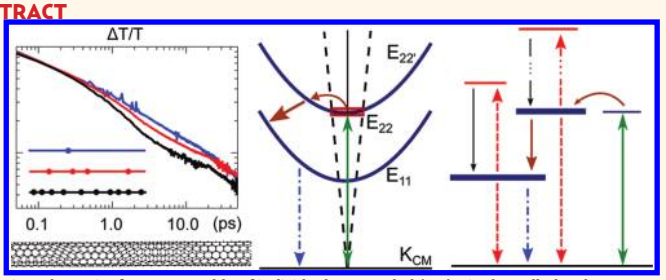

The exciton dynamics for an ensemble of individual, suspended (6,5), single-walled carbon nanotubes revealed by single color E_{22} resonant pump−probe spectroscopy for a wide range of pump fluences are reported. The optically excited initial exciton population ranges from approximately 5 to 120 excitons per ∼725 nm nanotube. At the higher fluences of this range, the pump−probe signals are no longer linearly dependent on the pump intensity. A single, predictive model is described that fits all data for two decades of pump fluences and three decades of delay times. The model introduces population loss from the optically active zero momentum E_{22} state to the rest of the E_{22} subband, which is dark due to momentum selection rules. In the single exciton limit, the E_{11} dynamics are well described by a stretched exponential, which is a direct consequence of diffusion quenching from an ensemble of nanotubes of different lengths. The observed change in population relaxation dynamics as a function of increasing pump intensity is attributed to exciton−exciton Auger de-excitation in the E_{11} subband and, to a lesser extent, in the E_{22} subband. From the fit to the model, an average defect density $1/\rho = 150$ nm and diffusion constants $D_{11} = 4$ cm^2/s and $D_{22} = 0.2$ cm^2/s are determined.

KEYWORDS: single-walled carbon nanotubes · pump−probe · diffusion

Coulomb interactions in carbon nanotubes result in strongly bound excitons rather than free electron−hole pairs following optical excitation.[1,2] The exciton binding energies dominate even in a screened environment[1−5] over free electron−hole pairs.[6] The interplay between the one-dimensional (1D) structure of semiconducting carbon nanotubes and the strong Coulomb interaction leads to a mix of 1D and 0D-like, or molecular-like, behavior due to the resulting large exciton binding energies.[1,2,7,8] The 1D properties are manifested in electrical and thermal transport,[9] phonon dispersion,[10,11] and diffusion,[12−15] while the 0D behavior is apparent in dipole interactions such as Raman scattering[16] and linear absorption and emission.

The mix of the 1D physical structure with the excitonic nature of the optical excitation affects the corresponding optical quantum efficiency. A thermalized distribution of exciton momenta in the E_{11} subband[17,18] excludes radiative decay due to the momentum selection rules that block optical transitions to all but $K_{CM} \approx 0$ states.[19] This leads to an effective radiative lifetime in optical transitions that is orders of magnitude longer than one based on the intrinsic dipole coupling of the $K_{CM} \approx 0$ transition.[19]

Consequently, there has been considerable interest in the study of (mainly) nonradiative exciton population decay dynamics resulting from both time-resolved fluorescence[14,18,20−24] and pump−probe measurements.[22,25−30] The early work was performed on carbon nanotube ensemble samples where the results were harder to interpret due to questions about sample quality effects. For example, one report[31] on the 40 fs decay from the E_{22} band was later shown to be due to efficient energy transfer resulting from bundling with larger diameter or metallic nanotubes.[32−34] Information on such fast decay dynamics is of relevance and value for saturable absorber applications in pumped

* Address correspondence to harrah@bu.edu, swan@bu.edu.

Received for review September 19, 2011 and accepted November 11, 2011.

Published online November 11, 2011
10.1021/nn203604v

lasers[35] but yields little information on the intrinsic relaxation of E_{22} excited nanotubes. Futhermore, there is much interest in increasing the photoluminescence quantum yield, for example, for carbon nanotube sensing applications.[36,37]

Even for high quality, homogeneous samples, such as the canonical (6,5) single-walled carbon nanotubes from the gradient ultacentrifugation method,[38] contradictory results are reported. For example, in recent work by Lanzani and co-workers, evidence of weak exciton−exciton annihilation in the (6,5) E_{11} level at concomitant high exciton density[28] is found. On the other hand, groups also working with pure ensembles observe very strong E_{11} exciton−exciton annihilation.[22,25] On the single tube level, coincidence measurements below 40 K showed a significant degree of photon antibunching, indicative of single exciton occupation of the E_{11} level.[39] Single, long, suspended nanotubes at room temperature exhibited photoluminescence saturation at ~2−3 excitons in the E_{11} band.[24]

In this study, the single-color E_{22} resonant pump−probe measurements of a near pure solution of (6,5) carbon nanotubes[38] are reported. The transient differential transmission signal $\Delta T/T$ is measured both in the nearly single exciton and the high exciton density saturation regimes and a complex, pump-fluence dependent decay behavior is observed. While the excitonic nature of optical excitations in carbon nanotubes is by now well established, its consequences have not been fully accounted for in modeling decay dynamics of the pump−probe kinetics. An exciton population decay model that fits all explored fluences and time delays for the observed large dynamic ranges reported here is achieved by including two physically important processes. Diffusion from the zero center-of-mass exciton momentum ($K_{CM} = 0$) into the full E_{22} exciton band dispersion is treated as an explicit population loss mechanism. In addition, it is necessary to include the effect of diffusion-limited defect quenching in an ensemble that results in a distribution of length-dependent decay rates and is modeled with a stretched exponential of fixed stretch exponent $\beta = {}^1/_2$. Finally, the pump−probe data for four of the experimental fluences is fit with a single set of time-constants, with the onset of exciton interactions fully accounted for by the increase in the known initial exciton density. To test the predictive power of this description, the resulting best-fit model and parameters are compared to two additional pump fluence signals and excellent agreement with these observed responses is obtained.

RESULTS AND DISCUSSION

Differential Pump−Probe Transmission Measurements. The change in the transmission intensity of a weak probe pulse due to a spatially overlapped pump pulse is described by the unitless quantity, $\Delta T(\tau)/T_0$. Here, τ is the time delay between pump and probe beams, $\Delta T(\tau)$ is the difference in the transmission of the probe power at a detector after the sample, in the absence (T^{pr}_{off}) and presence (T^{pr}_{on}) of the pump ($\Delta T = T^{pr}_{on}(\tau) - T^{pr}_{off}(\tau)$) and T_0 is just T^{pr}_{off}. The $T^{pr}_{on}(\tau)$ signal depends on the difference between the ground state and E_{22} populations. Hence, even though only the transition from the ground state to the E_{22} level is dipole coupled to the probe pulse, the population dynamics in the intermediate states $n_I(\tau)$ are probed *via* the ground state recovery contribution to the responses observed in this one-color study, with $\Delta T(\tau)/T_0 \propto 2n_{22}(\tau) + n_I(\tau)$. Therefore we need to consider all the intermediate level dynamics in order to describe the observed E_{22} pump−probe signals. We do not directly probe the E_{11} level population, but the proposed kinetic scheme is consistent with descriptions of E_{11} dynamics from previous work on single nanotubes[18,40] and ensembles.[20,25,41] The resulting model (see below) fits the observed responses at all fluences and for both short and long times.

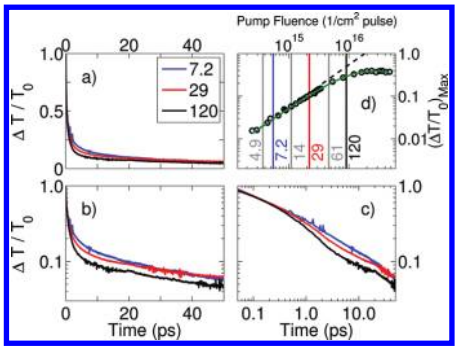

Figure 1. Observed E_{22} resonant pump−probe responses of (6,5) SWNTs for the indicated range of initial exciton population per nanotube. The responses have been normalized to the peak of the signal bleach for the range of pump fluences shown here. The signal is presented in (a) linear, (b) semilog, (c) log−log plots. (d) Observed $(\Delta T/T_0)_{MAX}$ resonant pump−probe responses of (6,5) SWNTs *versus* pump pulse fluences. The pump fluences used in this study are marked with the initial exciton population per nanotube. Note that the pump fluence range extends from the linear pump response regime to the onset of saturation.

The E_{22} pump−probe measurements were observed out to 50 ps. This time scale covers decay relaxation from the E_{22} level at the shortest times to the slower decays primarily associated with exciton diffusion-limited quenching in E_{11}. However, this time regime is not long enough to see the slower decay, on the order of hundreds of picoseconds, expected for dark excitons.[18]

Pump−probe responses at six different pump fluences between 2×10^{14} and 9.1×10^{15} photons/cm^2 were obtained. This range of fluences is significant because it covers both the low exciton density regime, where the transient response is linear with pump fluence, as well the high exciton density regime, where the observed signal exhibits saturation-like behavior[30] as shown in Figure 1d. The pump fluences for the pump−probe data are indicated in the figure.

We have previously measured the scattering and extinction to determine the average E_{22} transition dipole moment for this sample.[30] For the average nanotube length of 725 nm and measured absorption cross-section of 1.3×10^{-14} cm^{-2}, the experimental range of pump fluences used here corresponds to an initial excitation of 5 to 120 excitons per nanotube or an initial exciton density of 7 to 165 excitons/μm. The calculation of the initial exciton population averages over the random orientation of the nanotubes and the perpendicular orientation of the pump and probe pulses.[30] The limitations of this averaging in the presence of nonlinear decay are discussed later. The kinetic model presented below is convolved with a 54 fs Gaussian pulse autocorrelation in order to fit the observed interaction with the 38 fs pump and probe pulses.

To get a qualitative sense of the dynamics, the observed normalized pump−probe signals are plotted in different formats in Figure 1 (a) linear, (b) semilog, and (c) log−log plots up to 50 ps. Qualitatively, the data show a fast early decay and a much slower relaxation component attributed to ground state recovery at all pump fluences. From the linear plot, it is difficult to discern further qualitative information. However, the semilog plot shows that the signals cannot be uniformly described by a single or biexponential decay. The semilog plot emphasizes the longer delay times where the different fluences from 10−50 ps seem to exhibit a similar behavior. The log−log plot reveals that the observed kinetics do not obey a power-law temporal dependence and demonstrate the onset of a different behavior at higher fluences in the 1−10 ps regime. This high-fluence behavior is attributed to Auger decay in accordance with previous studies that have identified exciton−exciton annihilation as an important nonlinear decay mechanism for excitons in the E_{11} subband.[20,25,26] On the other hand, exciton−exciton annihilation does not appear to be important at the very shortest time scales (<1 ps). The observed pump−probe responses are independent of pump fluence during the first ~300 fs, as shown in Figure 1c. Hence, the data indicate that while increasing pump intensities affect the population dynamics at later times, there is no fluence induced increase in the rate of population loss in the first ~300 fs, and hence no significant Auger decay in the initially excited E_{22} level. Exciton Auger decay has been attributed as the cause for signal saturation with increasing pump fluence in studies probing the relaxation dynamics of the E_{11} band. For the E_{22} subband we have previously shown that the observed pump−probe saturation behavior is due to exciton-induced increase of the pure dephasing rate.[30]

Low Fluence Regime. In constructing a model for the E_{22} excited exciton population decay dynamics, we first discuss the low exciton density regime (noninteracting excitons), starting with short delay times. As illustrated in Figure 2b, we separate the E_{22} subband into optically accessible (bright) and inaccessible (dark) momentum states, labeled E_{22} and $E_{22'}$, respectively. Owing to momentum selection rules, the incident light can only excite and interact with excitons with nearly zero momentum (red box). When the remaining E_{22} subband ($E_{22'}$) states are populated from these initial excitons *via* thermalization, the probe bleach signal decreases due to this population loss from the bright $K_{CM} \approx 0$ state. Treating optically inaccessible (dark) E_{22} excitons separately from optically accessible (bright) excitons is necessary to fit the transient absorption dynamics during first decade of data (up to 500 fs). This separation into near-zero and nonzero momentum states is directly attributable to the excitonic nature of the optical excitations.[19]

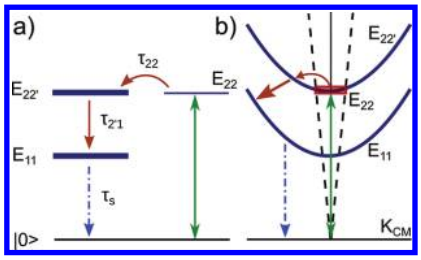

Figure 2. (a) The low fluence model used to fit the data. The green arrow represents the pump−probe interaction. Brown solid arrows are simple exponential decays and the blue dash-dotted arrow represent a stretched exponential decay due to decay at defects reached by diffusion. The thick lines $E_{22'}$ and E_{11} signify the thermalized E_{ii} subbands that are dark to the E_{22} probe, while the sharp line at E_{22} signifies the $K_{CM} \approx 0$ states. The difference in energy between E_{22} and $E_{22'}$ is well within the thermal energy and the transfer from E_{22} to $E_{22'}$ is mediated by phonons. (b) Schematic illustration of the structure of the excitonic bands and the light cone (dashed straight lines). The negligible momentum of the exciting light limits the optically accessible states to $K_{CM} \approx 0$ (E_{22}). All other states in the E_{22} subband ($E_{22'}$) are strictly dark even though their energy may overlap with the probe energy. The arrow from $E_{22'}$ to E_{11} signifies the exponential phonon mediated decay, followed by thermalization and diffusion in the E_{11} subband with subsequent defect quenching.

The efficient decay from the $E_{22'}$ subband to the E_{11} subband is attributed to a phonon mediated process.[42] Hence, the decay from $E_{22'}$ to E_{11} is modeled as a simple exponential decay. The E_{11} population dynamics have been probed directly previously with one and two-color E_{11} and E_{22} pump−probe studies,[25,26,28] and time-resolved photoluminescence[17] and has shown a complex relaxation behavior in ensemble studies even with a predominantly single chirality sample.[27,28] For nanotubes with low optical quantum yield, previous studies have identified exciton diffusion to defects as a dominant decay mechanism in the E_{11} subband.[12,14,43] For a single, defect-free nanotube at low fluence, this mechanism approximately produces a single exponential decay.[15,18] However, the decay time for diffusion-limited decay is a function of nanotube length.[15] The sample used in this study is an ensemble of nanotubes with a distribution of

lengths (Figure 3) and likely has quenching defects, which results in a distribution of decay times. The decay from an infinitely long nanotube with random quenching defects of a particular defect density ρ is equivalent to an ensemble of defect-free nanotubes with quenching ends and different lengths. Each nanotube length in the ensemble corresponds to the distance between two adjacent defects in the infinitely long nanotube and the average length in the ensemble is the same as the average distance between defects $\bar{l} = 1/\rho$ in the infinite nanotube. When defects are randomly located in the infinite nanotube, the lengths in the ensemble have an exponential probability distribution. Such a length distribution gives rise to a probability distribution of decay times that can be modeled by a stretched exponential $n(t) \propto \exp(-(t/\tau_s)^{\beta})$ with stretch exponent $\beta = {}^1/_2$.[14,15] Even samples prepared with density gradient ultracentrifugation[38] have been shown to have low quantum yields (~1%[44]) so that the radiative decay can be ignored[14,15] relative to the nonradiative decay mechanisms. The stretch time constant can be expressed as $\tau_s = \pi/(8D\rho^2)$ where D is the diffusion constant and ρ is the defect density.[45] The existence of a distribution of finite nanotube lengths in our sample skews this stretched exponential toward faster decay times. However, if the average distance between defects is shorter than the average length of the nanotubes, as we presume is the case for our sample due to the processing steps involved, the random defects dominate and the effect of the nanotube length distribution is less important. Parameters derived from these modeled pump–probe kinetics, discussed below, further justify this assumption.

Hence, we have a model for the low fluence regime (where exciton–exciton interactions can be ignored) as shown in Figure 2. The pump excites excitons into the optically accessible E_{22} state, followed by depopulation *via* a simple exponential decay (thermalization onset) into the $K_{CM} \neq 0$ $E_{22'}$ subband. From $E_{22'}$, a simple exponential decay takes the exciton into the E_{11} band. Finally, diffusion-limited quenching at defects and nanotube ends cause the ground state recovery of excitons from E_{11}. Owing to the distribution of lengths and existence of defects, this is modeled as a stretched exponential. We do not include an E_{11} dark exciton subband[46] because all of our attempts at modeling show that it is not relevant up to the 50 ps time delay in this study (see discussion below).

The absorption spectrum[30] shows a significant background level at the E_{22} energy. This background, which is discussed later, is modeled as an independent two-level system that is optically accessible by the pump and probe. Its contribution to the signal is kept in plots of the data and fits.

Low and High Fluence Model. In the high fluence regime, exciton–exciton interactions are expected to be important[20,24−26,41] as suggested by the different form of the pump–probe responses seen with increasing

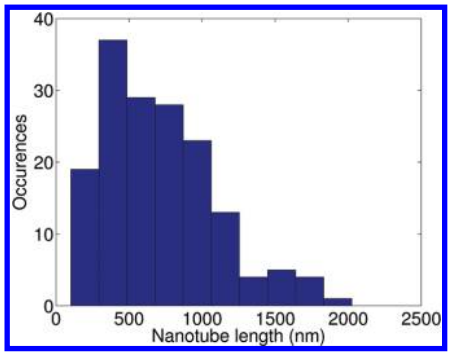

Figure 3. Length distribution measured by AFM. The length distribution can be approximated by a log-normal distribution with a mean of 725 nm, median of 610 nm, and mode of 435 nm.

pump fluence in Figure 1a–c. Auger recombination in both E_{11} and $E_{22'}$ but not in E_{22} are allowed in the proposed exciton decay model. This is justified because no population decay rate change at early times is observed as a function of pump fluence. Further, E_{22} is defined to be $K_{CM} \approx 0$, that is, stationary excitons are initially optically generated by the pump, and a diffusion-mediated exciton–exciton interaction cannot occur. In the E_{11} and $E_{22'}$ subbands, an excited exciton is promoted to a corresponding higher level *via* Auger annihilation and subsequently returns to the original subband. For example, in an Auger recombination in E_{11}, one exciton gets promoted to a higher energy level X_{11} and one relaxes to the ground state. From X_{11}, the exciton returns to E_{11}. The physical origin of the X_{ii} levels is not specified in the model. It is not possible to distinguish between the diffusive ($dn/dt = kt^{-1/2}n^2$),[22,47,48] coherent ($dn/dt = kn^2$),[17,22,25,48] and free particle ($dn/dt = kn^3$)[22,41] Auger decay mechanisms based on goodness of fit alone. The free particle mechanism is considered unlikely because optical transitions in nanotubes involve strongly bound excitonic states (0.3–0.4 eV).[1,2] The coherent Auger decay in E_{11} can also be ruled out since excitons created in E_{22} should not retain any coherence in $E_{22'}$ or E_{11}. This situation might very well be different for E_{11} pump–probe experiments,[48] where coherence times have been shown to exceed 100 fs even at room temperature.[49] Hence, on the basis of the known exciton diffusion to defects[12,14] decay pathway, and eliminating the other models on physical grounds, we selected the diffusive exciton–exciton annihilation as the most likely mechanism in agreement with recent work.[48] The full model for all fluences and times is shown in Figure 4a; the corresponding rate equations are presented in the Supporting Information.

This model describes the data across a wide range of fluences and at short and long time scales as demonstrated by the fit to the data shown in Figure 5 and Figure 6. We selected four of the six fluences for fitting, constraining the model parameters to be the same for each fluence. This global fitting procedure

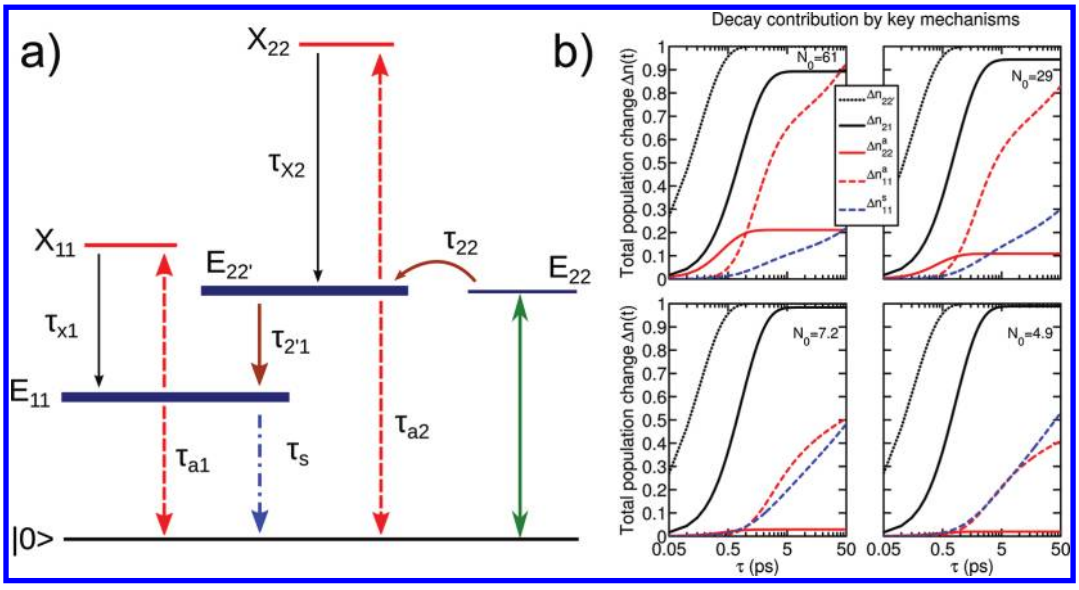

Figure 4. (a) The main model used to fit the data in Figure 5 and Figure 6. The green arrow represents the excitation to and stimulated emission from the E_{22} $K_{CM} = 0$ state. Red dashed arrows indicate exciton−exciton annihilation, black and brown solid arrows are simple exponential decays, and the blue arrow is a stretched exponential decay due to decay at defects reached by diffusion. Red horizontal lines indicate the state of the promoted exciton. Blue horizontal, thick lines are the part of the standard nanotube excitonic subbands that are thermally accessible. (b) Total population decay due to the main decay mechanisms in E_{22} (dotted lines), $E_{22'}$ (solid lines), and E_{11} (dashed lines) for different initial exciton populations N_0 (excitons/nanotube) marked in the upper right corners. The decay is normalized by the initial exciton population per nanotube to compare the relative importance of each mechanism for each fluence. The normalized population changes are $\Delta n_{22'}$ due to exponential decay from E_{22} into the $E_{22'}$ subband, Δn_{21} due to exponential decay from $E_{22'}$ to E_{11}, $\Delta n^a_{22'}$ due to the Auger decay in $E_{22'}$, Δn^a_{11} due to Auger rate in E_{11}, and Δn^s_{11} from diffusion quenching in E_{11}.

uses the same values for fit parameters for all fluences, with only the known initial exciton population depending on fluence. The low-fluence fit parameters are the simple exponential decay times τ_{22} from E_{22} to $E_{22'}$ and $\tau_{2'1}$ from $E_{22'}$ to E_{11} and the time constant τ_s for the stretched exponential. Rather than using the stretch exponent β as a fit parameter, we fixed it to $\beta = {}^1/_2$ to correspond to diffusion-limited quenching in E_{11}. The parameters associated with the Auger recombination processes are the E_{22} Auger rate k_{a2}, the X_{22} return time constant τ_{X2}, the E_{11} Auger rate k_{a1}, and the X_{11} return time constant τ_{X1}. The fluence dependence is represented in the initial exciton population, which is known from our previous work to be on average 4.9, 7.2, 14, 29, 61, and 120 excitons/nanotube[30] for the pump fluences studied here.

The initial populations used for fitting were 4.9, 7.2, 29, and 61 excitons/nanotube (Figure 5 and Figure 6). Without further fitting, we used the parameters from these fits to calculate the expected pump−probe decay responses for the remaining two fluences (Figure 7), which corresponded to initial exciton populations of 14 and 120 excitons/nanotube. An initial population of 120 excitons/nanotube is well into the saturation region, whereas 14 excitons/nanotube is in the middle of the populations used for fitting. That the fit works well for both the high and intermediate pump fluences verifies that the model captures the main dynamics without extraneous components and that each decay mechanism is physically justified and necessary. We have not let the stretch exponent β vary, which would otherwise be an easy way to have a better fit of the data without gaining useful physical information.

The resulting best fitted decays are displayed in Figure 5 and Figure 6. Many models appeared to fit the observed responses equally well when displayed in a linear plot, but the log−log plot format was found to be especially useful for evaluating trends in the residual and for discriminating between different models. The residuals in Figure 5 and Figure 6 demonstrate very good fits across all fluences and time scales. The structure in the residual that develops at higher fluences does not get worse when applying the fit to the highest fluence as shown in Figure 7.

The resulting values for the fit parameters are $\tau_{22} \approx 160$ fs, $\tau_{2'1} \approx 0.8$ ps and the time constant for the stretched exponential $\tau_s \approx 24$ ps. The parameters associated with the Auger recombination processes have decay rates k^a that are exciton density dependent with the E_{22} Auger time constant $k_{a2} = 0.15$ nm/fs$^{1/2}$, and the E_{11} Auger time constant $k_{a1} = 0.67$ nm/fs$^{1/2}$.

There are several key features of this model. The pump and probe beams interact with the optically accessible excitons in E_{22}. Thus, the initial exciton population comprises excitons with near zero momentum. The fast (~160 fs) transfer populates the thermally accessible E_{22} subband, ($E_{22'}$ in the figure)

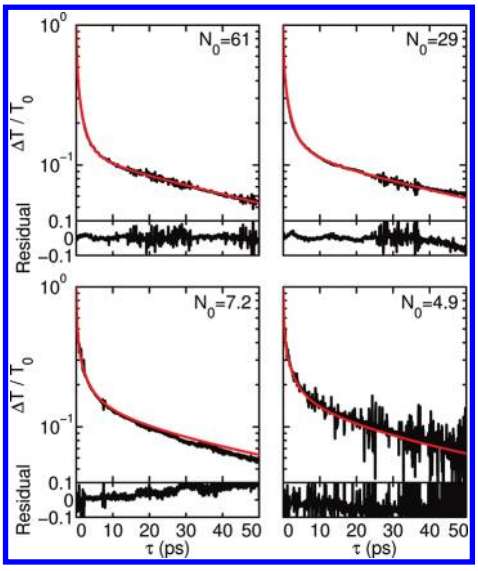

Figure 5. Semilog plot of transient absorption (black) for the initial exciton populations per nanotube indicated in the upper right corners. Fit using the model in Figure 4a (red). The residual is defined as (fit(τ) − data(τ))/(data(τ)).

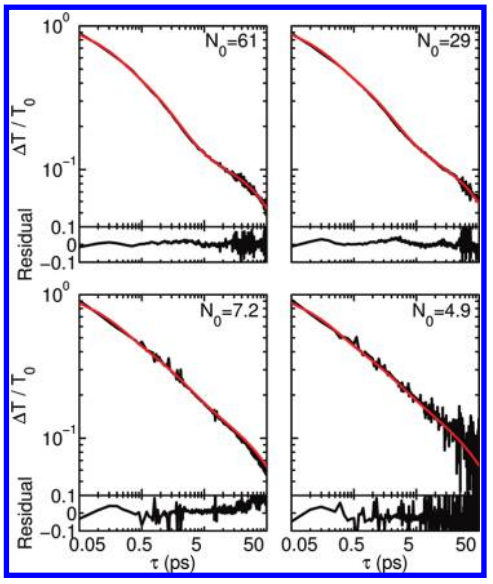

Figure 6. Log−log plot of transient absorption (black) for the initial exciton populations per nanotube indicated in the upper right corners. Fit using the model in Figure 4a (red). The residual is defined as (fit(τ) − data(τ))/(data(τ)).

and is ∼4 times slower than E_{22} (K_{CM} = 0) dephasing time.[30]

The decay from $E_{22'}$ to E_{11} is 0.8 ps, which is much longer than the often quoted 40 fs from an earlier study from 2005.[31] However, it has been shown that the presence of small bundles in such samples exhibits fast decay rates (∼10 fs).[32]

A number of different model variations, including changes in the type of decay (exponential, diffusion-limited quenching, or Auger) and adding or removing levels, are discussed in the Supporting Information. We find that the fast exponential decay out of E_{22} is a consistent mechanism in these variations with a short time constant (∼100−200 fs). Likewise the $E_{22'}$ decay is also consistent as an exponential decay with time constant of ∼0.5−2 ps. Diffusion-limited quenching is only necessary to describe decay in E_{11}, with a time constant of tens of picoseconds, and not in E_{22}. In agreement with previous studies[25,26,29] the Auger decay out of E_{11} is always an important ingredient, with a rate constant similar to that determined in the previous studies.[28]

The Auger processes and the single exciton diffusion quenching are both diffusion-based mechanisms for exciton population relaxation. From the fitted parameters for the two Auger decays and the stretched exponential decays, the diffusion constant D and the defect density ρ can be estimated. The decay for diffusive exciton−exciton annihilation takes the form of $dn/dt = k_a t^{-1/2} n^2(t)$, where $k_a = (\pi D/2)^{1/2}$ is a fit parameter in the model.[45] For the E_{11} and E_{22} subbands, the fitted parameters result in $D_{11} = 4$ cm^2/s and $D_{22} = 0.2$ cm^2/s, respectively.

The above results together with the stretch time constant can be used to determine ρ. Decay by stretched exponential has the form $dn/dt = (d/dt)\exp(-(t/\tau_s)^{\beta})$, with fit parameter $\tau_s = \pi/(8D\rho^2)$. Taking the D_{11} determined by the Auger decay contribution to the observed pump−probe responses and the corresponding fitted value τ_s = 24 ps, a defect density $1/\rho \approx 150$ nm is computed. This is well short of the 725 nm average nanotube length, *a posteriori* justifying the use of a stretched exponential. Nearly identical results (∼120 nm defect separation) have been deduced from a photoluminescence quantum yield study by Hertel *et al.*[14] on a (6,5) sample prepared by the same methods.[38] The E_{11} diffusion constant of 4 cm^2/s is within the range of previous calculations and experiments, (0.2−11 cm^2/s).[14,23,43,50,51] The value of D for E_{22} is expected to be shorter than that of E_{11} because of the larger effective mass of the E_{22} excitons than the E_{11} excitons, and the much faster dephasing time.[30] These differences yield a smaller D because $D \propto \tau_{ph}/m^*$, where τ_{ph} is the mean free path time and is assumed to be roughly proportional to the dephasing time. This expected relationship between the diffusion constants is consistent with the 0.2 cm^2/s diffusion constant that we obtain for E_{22} being smaller than the 4 cm^2/s value we obtain for E_{11}.

The resulting normalized integrated decay rates are plotted in Figure 4b for decay from the E_{22} (dotted line), $E_{22'}$ (solid lines), and E_{11} levels (dashed lines). The integrated decay rate gives the total number of excitons that have decayed by a particular decay mechanism by a given time. Decay rates are given for initial exciton populations of 61, 29, 7.2, and 4.9 excitons/nanotube in this figure. One can see how the Auger decays increase in significance for the higher fluences. The figure shows how E_{22}, the only directly probed state above the ground state, is essentially

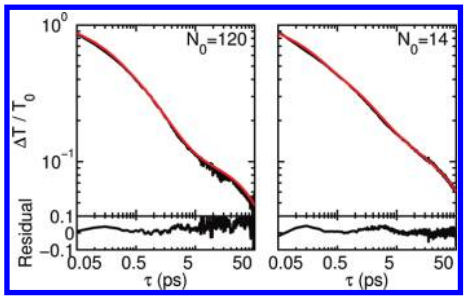

Figure 7. Log−log plot of transient absorption (black) for the initial exciton populations per nanotube indicated in the upper right corners and plotted with the model in Figure 4a using the parameters from the fit in Figure 6 (red). The residual is defined as (fit(τ) − data(τ))/(data(τ)).

emptied out in the first ~500 fs. The relative importance of the decay mechanisms from the two intermediate states to the observed pump−probe responses is shown by the solid lines and dashed lines. The depopulation of $E_{22'}$ is complete after 5 ps. $E_{22'}$ Auger contribution is only noticeable at the highest initial exciton populations. The most striking feature in these relative decays is the strength of the E_{11} Auger decay. The last decade of the pump−probe kinetics, 5−50 ps is dominated by the E_{11} decay dynamics contribution to the ground state recovery. The reason that the normalized number of excitons leaving E_{11} is sometimes greater than 1 is because half of the excitons from Auger decay return to E_{11} and therefore leave the band more than once. The strong E_{11} inelastic exciton interactions are consistent with previous studies[49,52] and sets a limit on the number of excitons that can exist in E_{11}.[47]

Model Discussion. The model summarized in Figure 4a successfully fits the observed E_{22}-resonant pump−probe responses at all measured fluence regimes and time scales. However, some minor deviations can be seen in the residuals in Figure 6 and Figure 7. Because nonlinear processes contribute to the model, assumptions based on average quantities may not be strictly accurate. For example, to account for the isotropic nanotube orientations, the initial pump-pulse induced exciton population is averaged over all orientations.[30] The pump and probe pulses are orthogonal, so nanotubes with the highest initial exciton population will have weaker interaction with the probe pulse. Similarly, the nanotubes with lower initial population will interact more strongly with the probe pulse. We therefore have a distribution of populations, which will skew the nonlinear decay rates determined by the model.

The possibility of an E_{11} dark exciton subband below the bright exciton subband[46] was considered in this modeling analysis. The transfer rates between the bright and dark states were taken as fit parameters. Variations on this base model, including using the dark level either as a shelving state or allowing diffusion quenching of the dark excitons, did not result in physically reasonable fit values. Attempts at fitting the observed pump−probe responses with this alternative model are discussed in Supporting Information. The lack of influence of a dark state could be due to several reasons. Time resolved measurements[18] have shown that dark states have decay times of several hundreds of ps, much longer than the 50 ps time scale probed here. In addition, at room temperature, the typically small energy separation between the bright and dark states of order 1 meV makes the dark states less important.[53,54]

An effective additional relaxation pathway from the initial excited state to the ground state is robustly obtained by this fitting procedure that we attribute to background absorption.[30] The early, subpicosecond signal cannot be fit accurately without a rapid depopulation of the initial excited state and repopulation of the ground state. If we consider this to be an E_{22} excitation with a fast path directly to the ground state, it would mean a very fast decay rate from the E_{22} level with subpicosecond time scale. Because there are no known physical processes that would produce such a fast decay, this explanation for the relaxation seems highly unlikely. Instead the fast decay is attributed to a separate channel for rapid relaxation to the ground state. The absorption spectrum[30] shows a significant background level that could be responsible for such an extra rapid decay channel.

CONCLUSION

Single-color pump−probe measurements on suspended, isolated (6,5) carbon nanotubes due to 38 fs laser pulses resonant with the E_{22} excitonic transition are reported. A comprehensive model is developed that is able to describe the transient transmission of an ensemble sample of nanotubes over several orders of magnitude of pump fluences and decay time scales. The same set of model parameters are found to provide excellent fits to the observed decay for all pump fluences once the known initial exciton populations are specified. A unique feature of this analysis is the population decay from the optically active $K_{CM} \approx 0$ state of the exciton to the $E_{22'}$ subband continuum—a direct consequence of the strong exciton binding in these systems. The simple exponential phonon mediated decay from the $E_{22'}$ subband to the E_{11} subband is $\tau_{2'1} \approx 0.8$ ps, significantly slower than stated previously.[31] A weak exciton−exciton annihilation in the $E_{22'}$ subband is necessary to fit the data at higher fluences. On the other hand, the ground state recovery from the E_{11} subband is dominated by the 1D nature of the nanotubes. Diffusion quenching *via* ends or defects results in a stretched exponential decay, and the E_{11} subband diffusive exciton−exciton interactions are comparable or stronger than the diffusion decay for all explored fluences. The E_{11} Auger results are consistent with other work demonstrating exciton−exciton annihilation and diffusion-limited quenching of E_{11}

excitons.[12,20] Analysis of the diffusion-related decay rates gives values of defect density $1/\rho = 150$ nm and diffusion constants of E_{11} equal to 4 cm^2/s and of E_{22} equal to 0.2 cm^2/s.

METHODS

The enriched nanotube sample consisting of predominantly (6,5) single-walled carbon nanotubes was produced using density gradient ultracentrifugation.[38] The final (6,5) enriched material was dialyzed into 1% w/v sodium cholate aqueous solution to remove the density gradient medium (iodixanol). The nanotubes' length distribution was measured by multiple AFM images and can be approximated by a log-normal distribution with an average length of 725 nm (Figure 3). The density of carbon nanotubes in the sample is $\sim 1.6 \times 10^{14}$ cm^{-3}. For more details about the sample, see an earlier work.[30]

Ultrafast pulses with a central wavelength of 571 nm, resonant with E_{22} were produced by an optical parametric amplifier pumped by a 100 kHz Ti:sapphire regenerative amplifier system. One-color pump−probe measurements were performed with near transform-limited Gaussian pulses of 38 fs pulse width, corresponding to a spectral width of 52 meV (420 cm^{-1}). The probe and pulse beams were orthogonally polarized in order to minimize pump scatter contamination along the probe direction and coherence coupling effects at the earliest times. A polarizer and half-wave plate combination was used to achieve the large dynamic range of incident pump pulse fluences used here. For additional experimental details, see an earlier work.[30]

Acknowledgment. We thank S. Redner, T. Hertel, and A. Walsh for helpful discussions. D.M.H. and A.K.S. acknowledge funding from the National Science Foundation (DMR-0706574). J.R.S. and L.D.Z. acknowledge funding from the NSF (CHE-0310497) and the support of the Boston University Photonics Center. MCH and AAG acknowledge funding from the NSF (DMR-0520513, EEC-0647560, DMR-1006391) and the Nanoelectronics Research Initiative. A.A.G. acknowledges a Natural Sciences and Engineering Research Council of Canada Postgraduate Scholarship.

Supporting Information Available: Rate equations, fit parameter values, and discussion of alternative models. This material is available free of charge *via* the Internet at http://pubs.acs.org.

REFERENCES AND NOTES

1. Maultzsch, J.; Pomraenke, R.; Reich, S.; Chang, E.; Prezzi, D.; Ruini, A.; Molinari, E.; Strano, M. S.; Thomsen, C.; Lienau, C. Exciton Binding Energies in Carbon Nanotubes from Two-Photon Photoluminescence. *Phys. Rev. B* **2005**, *72*, 241402.
2. Wang, F.; Dukovic, G.; Brus, L. E.; Heinz, T. F. The Optical Resonances in Carbon Nanotubes Arise from Excitons. *Science* **2005**, *308*, 838–841.
3. Perebeinos, V.; Tersoff, J.; Avouris, P. Scaling of Excitons in Carbon Nanotubes. *Phys. Rev. Lett.* **2004**, *92*, 257402.
4. Choi, J. H.; Strano, M. S. Solvatochromism in Single-Walled Carbon Nanotubes. *Appl. Phys. Lett.* **2007**, *90*, 223114.
5. Walsh, A. G.; Vamivakas, A. N.; Yin, Y.; Cronin, S. B.; Unlu, M. S.; Goldberg, B. B.; Swan, A. K. Screening of Excitons in Single, Suspended Carbon Nanotubes. *Nano Lett.* **2007**, *7*, 1485–1488.
6. Vamivakas, A. N.; Walsh, A.; Yin, Y.; Unlu, M. S.; Goldberg, B. B.; Swan, A. K. Exciton-Mediated One-Phonon Resonant Raman Scattering from One-Dimensional Systems. *Phys. Rev. B* **2006**, *74*, 205405.
7. Spataru, C. D.; Ismail-Beigi, S.; Benedict, L. X.; Louie, S. G. Excitonic Effects and Optical Spectra of Single-Walled Carbon Nanotubes. *Phys. Rev. Lett.* **2004**, *92*, 077402.
8. Capaz, R. B.; Spataru, C. D.; Ismail-Beigi, S.; Louie, S. G. Diameter and Chirality Dependence of Exciton Properties in Carbon Nanotubes. *Phys. Rev. B* **2006**, 121401.
9. Deshpande, V. V.; Hsieh, S.; Bushmaker, A. W.; Bockrath, M.; Cronin, S. B. Spatially Resolved Temperature Measurements of Electrically Heated Carbon Nanotubes. *Phys. Rev. Lett.* **2009**, *102*, 105501.
10. Souza Filho, A. G.; Jorio, A.; Dresselhaus, G.; Dresselhaus, M. S.; Saito, R.; Swan, A. K.; Unlu, M. S.; Goldberg, B. B.; Hafner, J. H.; Lieber, C. M.; *et al.* Effect of Quantized Electronic States on the Dispersive Raman Features in Individual Single-Wall Carbon Nanotubes. *Phys. Rev. B* **2001**, *65*, 035404.
11. Rafailov, P. M.; Maultzsch, J.; Thomsen, C.; Dettlaff-Weglikowska, U.; Roth, S. Kohn Anomaly and Electron-Phonon Interaction at the K-Derived Point of the Brillouin Zone of Metallic Nanotubes. *Nano Lett.* **2009**, *9*, 3343−3348, PMID: 19694489.
12. Cognet, L.; Tsyboulski, D.; Rocha, J.-D. R.; Doyle, C. D.; Tour, J. M.; Weisman, R. B. Stepwise Quenching of Exciton Fluorescence in Carbon Nanotubes by Single-Molecule Reactions. *Science* **2007**, *316*, 1465.
13. Moritsubo, S.; Murai, T.; Shimada, T.; Murakami, Y.; Chiashi, S.; Maruyama, S.; Kato, Y. K. Exciton Diffusion in Air-Suspended Single-Walled Carbon Nanotubes. *Phys. Rev. Lett.* **2010**, *104*, 247402.
14. Hertel, T.; Himmelein, S.; Ackermann, T.; Stich, D.; Crochet, J. Diffusion Limited Photoluminescence Quantum Yields in 1-D Semiconductors: Single-Wall Carbon Nanotubes. *ACS Nano* **2010**, *4*, 7161–7168.
15. Harrah, D. M.; Swan, A. K. The Role of Length and Defects on Optical Quantum Efficiency and Exciton Decay Dynamics in Single-Walled Carbon Nanotubes. *ACS Nano* **2011**, *5*, 647–655.
16. Duque, J. G.; Chen, H.; Swan, A. K.; Shreve, A. P.; Kilina, S.; Tretiak, S.; Tu, X.; Zheng, M.; Doorn, S. K. Violation of the Condon Approximation in Semiconducting Carbon Nanotubes. *ACS Nano* **2011**, *5*, 5233–5241.
17. Wang, F.; Dukovic, G.; Brus, L. E.; Heinz, T. F. Time-Resolved Fluorescence of Carbon Nanotubes and Its Implication for Radiative Lifetimes. *Phys. Rev. Lett.* **2004**, *92*, 177401.
18. Berciaud, S.; Cognet, L.; Lounis, B. Luminescence Decay and the Absorption Cross Section of Individual Single-Walled Carbon Nanotubes. *Phys. Rev. Lett.* **2008**, *101*, 077402.
19. Spataru, C. D.; Ismail-Beigi, S.; Capaz, R. B.; Louie, S. G. Theory and *ab Initio* Calculation of Radiative Lifetime of Excitons in Semiconducting Carbon Nanotubes. *Phys. Rev. Lett.* **2005**, *95*, 247402.
20. Wang, F.; Dukovic, G.; Knoesel, E.; Brus, L. E.; Heinz, T. F. Observation of Rapid Auger Recombination in Optically Excited Semiconducting Carbon Nanotubes. *Phys. Rev. B* **2004**, *70*, 241403.
21. Hagen, A.; Steiner, M.; Raschke, M. B.; Lienau, C.; Hertel, T.; Qian, H.; Meixner, A. J.; Hartschuh, A. Exponential Decay Lifetimes of Excitons in Individual Single-Walled Carbon Nanotubes. *Phys. Rev. Lett.* **2005**, *95*, 197401.
22. Valkunas, L.; Ma, Y.-Z.; Fleming, G. R. Exciton−Exciton Annihilation in Single-Walled Carbon Nanotubes. *Phys. Rev. B* **2006**, *73*, 115432.
23. Miyauchi, Y.; Matsuda, K.; Yamamoto, Y.; Nakashima, N.; Kanemitsu, Y. Length-Dependent Photoluminescence Lifetimes in Single-Walled Carbon Nanotubes. *J. Phys. Chem. B* **2010**, *114*, 12905–12908.
24. Xiao, Y.-F.; Nhan, T. Q.; Wilson, M.W. B.; Fraser, J. M. Saturation of the Photoluminescence at Few-Exciton Levels in a Single-Walled Carbon Nanotube under Ultrafast Excitation. *Phys. Rev. Lett.* **2010**, *104*, 017401.
25. Ma, Y.-Z.; Valkunas, L.; Dexheimer, S. L.; Bachilo, S. M.; Fleming, G. R. Femtosecond Spectroscopy of Optical Excitations in Single-Walled Carbon Nanotubes: Evidence for Exciton- Exciton Annihilation. *Phys. Rev. Lett.* **2005**, *94*, 157402.

26. Huang, L.; Krauss, T. D. Quantized Bimolecular Auger Recombination of Excitons in Single-Walled Carbon Nanotubes. *Phys. Rev. Lett.* **2006**, *96*, 057407.
27. Zhu, Z.; Crochet, J.; Arnold, M. S.; Hersam, M. C.; Ulbricht, H.; Resasco, D.; Hertel, T. Pump−Probe Spectroscopy of Exciton Dynamics in (6,5) Carbon Nanotubes. *J. Phys. Chem. C* **2007**, *111*, 3831–3835.
28. Luer, L.; Hoseinkhani, S.; Polli, D.; Crochet, J.; Hertel, T.; Lanzani, G. Size and Mobility of Excitons in (6,5) Carbon Nanotubes. *Nat. Phys.* **2009**, *5*, 54–58.
29. Graham, M. W.; Chmeliov, J.; Ma, Y.-Z.; Shinohara, H.; Green, A. A.; Hersam, M. C.; Valkunas, L.; Fleming, G. R. Exciton Dynamics in Semiconducting Carbon Nanotubes. *J. of Phys. Chem. B* **2011**, *115*, 5201–5211.
30. Schneck, J. R.; Walsh, A. G.; Green, A. A.; Hersam, M. C.; Ziegler, L. D.; Swan, A. K. Electron Correlation Effects on the Femtosecond Dephasing Dynamics of E22 Excitons in (6,5) Carbon Nanotubes. *J. Phys. Chem. A* **2011**, *115*, 3917–3923.
31. Manzoni, C.; Gambetta, A.; Menna, E.; Meneghetti, M.; Lanzani, G.; Cerullo, G. Intersubband Exciton Relaxation Dynamics in Single-Walled Carbon Nanotubes. *Phys. Rev. Lett.* **2005**, *94*, 207401.
32. Luer, L.; Crochet, J.; Hertel, T.; Cerullo, G.; Lanzani, G. Ultrafast Excitation Energy Transfer in Small Semiconducting Carbon Nanotube Aggregates. *ACS Nano* **2010**, *4*, 4265–4273.
33. Koyama, T.; Asada, Y.; Hikosaka, N.; Miyata, Y.; Shinohara, H.; Nakamura, A. Ultrafast Exciton Energy Transfer between Nanoscale Coaxial Cylinders: Intertube Transfer and Luminescence Quenching in Double-Walled Carbon Nanotubes. *ACS Nano* **2011**, *5*, 5881–5887.
34. Koyama, T.; Asaka, K.; Hikosaka, N.; Kishida, H.; Saito, Y.; Nakamura, A. Femtosecond Luminescence Decay Due to Exciton Energy Transfer in Single-Walled Carbon Nanotube Bundles. *J. Lumin.* **2011**, *131*, 494–497.
35. Kelleher, E.; Travers, J.; Sun, Z.; Ferrari, A.; Golant, K.; Popov, S.; Taylor, J. Bismuth Fiber Integrated Laser Mode-Locked by Carbon Nanotubes. *Laser Phys. Lett.* **2010**, *7*, 790–794.
36. Heller, D. A.; Jin, H.; Martinez, B. M.; Patel, D.; Miller, B. M.; Yeung, T.-K.; Jena, P. V.; Hobartner, C.; Ha, T.; Silverman, S. K.; *et al*. Multimodal Optical Sensing and Analyte Specificity Using Single-Walled Carbon Nanotubes. *Nat. Nanotechnol.* **2009**, *4*, 114–120.
37. Duque, J. G.; Gupta, G.; Cognet, L.; Lounis, B.; Doorn, S. K.; Dattelbaum, A. M. New Route to Fluorescent Single-Walled Carbon Nanotube/Silica Nanocomposites: Balancing Fluorescence Intensity and Environmental Sensitivity. *J. Phys. Chem. C* **2011**, *115*, 15147–15153.
38. Arnold, M. S.; Green, A. A.; Hulvat, J. F.; Stupp, S. I.; Hersam, M. C. Sorting Carbon Nanotubes by Electronic Structure Using Density Differentiation. *Nat. Nanotechnol.* **2006**, *1*, 60–65.
39. Hogele, A.; Galland, C.; Winger, M.; Imamoglu, A. Photon Antibunching in the Photoluminescence Spectra of a Single Carbon Nanotube. *Phys. Rev. Lett.* **2008**, *100*, 217401.
40. Gokus, T.; Hartschuh, A.; Harutyunyan, H.; Allegrini, M.; Hennrich, F.; Kappes, M.; Green, A. A.; Hersam, M. C.; Araujo, P. T.; Jorio, A. Exciton Decay Dynamics in Individual Carbon Nanotubes at Room Temperature. *Appl. Phys. Lett.* **2008**, *92*, 153116.
41. Wang, F.; Wu, Y.; Hybertsen, M. S.; Heinz, T. F. Auger Recombination of Excitons in One-Dimensional Systems. *Phys. Rev. B* **2006**, *73*, 245424.
42. Perebeinos, V.; Tersoff, J.; Avouris, P. Radiative Lifetime of Excitons in Carbon Nanotubes. *Nano Lett.* **2005**, *5*, 2495–2499.
43. Rajan, A.; Strano, M. S.; Heller, D. A.; Hertel, T.; Schulten, K. Length-Dependent Optical Effects in Single Walled Carbon Nanotubes. *J. Phys. Chem. B* **2008**, *112*, 6211–6213.
44. Crochet, J.; Clemens, M.; Hertel, T. Quantum Yield Heterogeneities of Aqueous Single-Wall Carbon Nanotube Suspensions. *J. Am. Chem. Soc.* **2007**, *129*, 8058–8059.
45. Redner, S. *A Guide to First-Passage Processes*; Cambridge University Press: New York, 2007; p 272.
46. Zhao, H.; Mazumdar, S. Electron−Electron Interaction Effects on the Optical Excitations of Semiconducting Single-Walled Carbon Nanotubes. *Phys. Rev. Lett.* **2004**, *93*, 157402.
47. Murakami, Y.; Kono, J. Existence of an Upper Limit on the Density of Excitons in Carbon Nanotubes by Diffusion-Limited Exciton−Exciton Annihilation: Experiment and Theory. *Phys. Rev. B* **2009**, *80*, 035432.
48. Graham, M. W.; Chmeliov, J.; Ma, Y.-Z.; Shinohara, H.; Green, A. A.; Hersam, M. C.; Valkunas, L.; Fleming, G. R. Exciton Dynamics in Semiconducting Carbon Nanotubes. *J. Phys. Chem. B* **2011**, *115*, 5201–5211.
49. Ma, Y.-Z.; Graham, M. W.; Fleming, G. R.; Green, A. A.; Hersam, M. C. Ultrafast Exciton Dephasing in Semiconducting Single-Walled Carbon Nanotubes. *Phys. Rev. Lett.* **2008**, *101*, 217402.
50. Georgi, C.; Bohmler, M.; Qian, H.; Novotny, L.; Hartschuh, A. Probing Exciton Propagation and Quenching in Carbon Nanotubes with Near-Field Optical Microscopy. *Phys. Status Solidi B* **2009**, *246*, 2683–2688.
51. Siitonen, A. J.; Tsyboulski, D. A.; Bachilo, S. M.; Weisman, R. B. Surfactant-Dependent Exciton Mobility in Single-Walled Carbon Nanotubes Studied by Single-Molecule Reactions. *Nano Lett.* **2010**, *10*, 1595–1599.
52. Abramavicius, D.; Ma, Y.-Z.; Graham, M. W.; Valkunas, L.; Fleming, G. R. Dephasing in Semiconducting Single-Walled Carbon Nanotubes Induced by Exciton-Exciton Annihilation. *Phys. Rev. B* **2009**, *79*, 195445.
53. Srivastava, A.; Htoon, H.; Klimov, V. I.; Kono, J. Direct Observation of Dark Excitons in Individual Carbon Nanotubes: Inhomogeneity in the Exchange Splitting. *Phys. Rev. Lett.* **2008**, *101*, 087402.
54. Nish, A.; Nicholas, R. J.; Faugeras, C.; Bao, Z.; Potemski, M. High-Field Magnetooptical Behavior of Polymer-Embedded Single-Walled Carbon Nanotubes. *Phys. Rev. B* **2008**, *78*, 245413.1